This is a preprint, the final version is subject to change, of the American Mineralogist (MSA)
Cite as Authors (Year) Title. American Mineralogist, in press.
DOI: http://dx.doi.org/10.2138/am-2018-6083

REVISION 1

Leesite, $K(H_2O)_2[(UO_2)_4O_2(OH)_5]\cdot 3H_2O$, a new K-bearing schoepite-family mineral from the Jomac mine, San Juan County, Utah, USA.

Travis A. Olds[1*], Jakub Plášil[2], Anthony R. Kampf[3], Tyler Spano[1], Patrick Haynes[4], Shawn M. Carlson[5], Peter C. Burns[1,6], Antonio Simonetti[1], Owen P. Mills[7]

[1] Department of Civil and Environmental Engineering and Earth Sciences, University of Notre Dame, Notre Dame, IN 46556, USA
[2] Institute of Physics ASCR, v.v.i., Na Slovance 1999/2, 18221 Prague 8, Czech Republic
[3] Mineral Sciences Department, Natural History Museum of Los Angeles County, 900 Exposition Boulevard, Los Angeles, CA 90007, USA
[4] 901 Sean Street, Socorro, NM 87801, USA
[5] 245 Jule Lake Road, Crystal Falls, MI 49920, USA
[6] Department of Chemistry and Biochemistry, University of Notre Dame, Notre Dame, IN 46556, USA
[7] Applied Chemical and Morphological Analysis Laboratory, Michigan Technological University, Houghton, MI 49931, USA

*E-mail: tolds@nd.edu

ABSTRACT

Leesite (IMA2016-064), $K(H_2O)_2[(UO_2)_4O_2(OH)_5]\cdot 3H_2O$, is a new uranyl-oxide hydroxyl-hydrate found underground in the Jomac mine, Brown's Rim, White Canyon mining district, San Juan County, Utah. The new mineral occurs as aggregates of vitreous orange yellow tablets stacked on {100}, individually reaching up to 1 mm in diameter. Leesite is non-fluorescent under both LW and SW UV, is translucent with a light yellow streak, has approximate hardness of 2 (Mohs), and has brittle tenacity with uneven fracture. Crystals have perfect cleavage along {100}, and exhibit the forms {100}. Optically, leesite is biaxial (-), with $\alpha = 1.745(2)$, $\beta = 1.761(2)$, $\gamma = 1.765(2)$ (white light); $2V$ (meas.) = 50(2)°, $2V$ (calc.) = 52.7°; dispersion is $r > v$, strong. Pleochroism: X nearly colorless, Y and Z orange yellow; $X < Y \approx Z$. Laser Ablation Inductively Coupled Plasma Mass Spectrometry (LA-ICP-MS) analyses provided the empirical formula $K_{0.67}Na_{0.004}Ca_{0.012}U_4O_{20}H_{15.31}$, based on 4 U and 20 O *apfu*. Leesite is orthorhombic, *Pbca*, $a = 14.866(7)$, $b = 14.1267)$, $c = 16.772(8)$ Å, $V = 3522(3)$ Å^3 and $Z = 8$. The crystal

structure (R_1 = 0.062) for 1778 reflections with $I_{obs} > 4\sigma I$), consists of sheets of edge-sharing uranyl pentagonal bipyramids linked together through an interlayer populated by K^+ and (H_2O) molecules. Sheets in leesite adopt the fourmarierite anion topology, and so belong to the schoepite family of related structures that differ in the interlayer composition and arrangement, and charge of the sheet. Leesite may form as one of the principal components of "gummite" mixtures formed during the alteration of uraninite, and the unit cell of leesite resembles the previously described, but poorly understood mineral, paraschoepite. Uptake of dangerous radionuclides (^{90}Sr, ^{135}Cs, ^{137}Cs, ^{237}Np, ^{238}Pu) into the structure of leesite and other members of the family has important implications for the safe disposal of nuclear waste.

Running title: Leesite, a new mineral from Utah, USA

Keywords: Leesite, sheet anion topology, schoepite, uranium, uraninite, crystal structure

INTRODUCTION

Uranium dioxide nuclear fuel and uraninite, UO_{2+x}, readily alter in the presence of water and oxygen leading to the formation of uranyl-oxide hydroxyl-hydrate minerals (UOH) (Finch and Ewing, 1992; Wronkiewicz et al., 1992). UOH minerals are among the first phases to form during the oxidation-hydration weathering of UO_2 (Finch et al., 1996a; Plášil, 2014), and studies detailing their structure, solubility, and stability are numerous due to their importance for nuclear waste disposal and the environmental chemistry of uranium in general (Amonette et al., 1994; Finch and Murakami, 1999; Klingensmith et al., 2007; Kubatko et al., 2006). Schoepite, $[(UO_2)_8O_2(OH)_{12}](H_2O)_{12}$, the most hydrous UOH, was described by Walker (1923) nearly ninety-five years ago, yet the crystal-

chemical details of phases produced during its dehydration are still uncertain. Different minerals form depending on the rate of dehydration, and the presence of cations can impart variable (OH^-) content in the sheets that build UOH minerals (Table 1). The structures of several of these minerals are built from the same sheet topology found in schoepite (Finch et al., 1996b), and the so-named schoepite family includes schoepite, metaschoepite, $[(UO_2)_4O(OH)_6](H_2O)_5$, (Weller et al., 2000), fourmarierite, $Pb[(UO_2)_4O_3(OH)_4](H_2O)_4$, (Li and Burns, 2000), paraschoepite, $UO_3 \cdot 1.9H_2O$, (Schoep and Stradiot, 1947), paulscherrerite, $UO_2(OH)_2$, (previously "dehydrated-schoepite") (Brugger et al., 2011), and heisenbergite, $UO_2(OH)_2(H_2O)$, (Walenta and Theye, 2012). Describing the crystallography of these minerals has been challenging due to the lack of suitably pure material, in sufficiently large crystals. Leesite is a new member of the schoepite family containing monovalent cations in the interlayer and marks the 22nd addition to the family of uranyl-oxide hydroxyl-hydrate minerals. Plášil et al. (2016) give an updated listing of the members of this family. Herein, we provide a description of the crystal structure of leesite and observations regarding substitutional variability between other members of the family, including Na-rich metaschoepite, and K-rich fourmarierite from Jáchymov, Czech Republic.

The name leesite honors American mineral dealer and collector Bryan K. Lees (born 1957). Mr. Lees received his B.S. in Geological Engineering from the Colorado School of Mines in 1985. In the same year, he founded Collector's Edge Minerals, through which he has developed innovative specimen extraction techniques and created what is probably the world's most advanced collector-specimen preparation laboratory. In the 1990's, Lees spearheaded the mining of rhodochrosite at Colorado's Sweet Home mine. The rhodochrosite samples produced by this venture are widely considered to be some of

the most valuable non-gem mineral specimens ever found, and many were personally collected with his advanced extraction techniques. Lees has conducted 40 specimen-mining projects on five continents and his samples are displayed in the collections of museums and individuals around the world. For his accomplishments, he has received the Friends of Mineralogy Author of the Year Award (1998), Carnegie Mineralogical Award (1998), the Colorado School of Mines Medal (2003), and the American Mineral Heritage Award (2014).

The Commission on New Minerals, Nomenclature, and Classification of the International Mineralogical Association approved the new mineral and name (IMA2016-064). The description is based upon two cotype specimens from the Jomac mine, deposited in the Natural History Museum of Los Angeles County, 900 Exposition Boulevard, Los Angeles, California 90007, U.S.A., with catalogue numbers 66285 and 66286.

OCCURRENCE

Leesite is found underground in the Jomac mine, Brown's Rim, White Canyon mining district, San Juan County, Utah (37°51'43"N 110°19'10"W), about 5.5 km SE of Hite Crossing. Material containing the new mineral was collected in 1989 by one of the authors (P.H.). The Jomac mine consisted of three adits that are now closed and reclaimed. Collecting has been prohibited since 1992 when the area was incorporated into the Glen Canyon National Recreation Area. Leesite was found in a seam of gypsum, closely associated with compreignacite, $K_2[(UO_2)_6O_4(OH)_6](H_2O)_7$, and a later generation of blatonite, $UO_2CO_3 \cdot H_2O$, (Vochten and Deliens, 1998) and owsaldpeetersite, $(UO_2)_2CO_3(OH)_2 \cdot 4H_2O$ (Vochten et al., 2001), two minerals for which the Jomac mine is the type locality. Other accessory minerals include alunite, chalcoalumite, probable

mbobomkulite or nickelalumite, sklodowskite, and boltwoodite. The deposit of uranium exploited by the Jomac mine lies in the Shinarump conglomerate member of the Triassic Chinle Formation. An account of the geology and history of the mine is given by Trites and Hadd (1958). Haynes (2000) summarizes this paper, and includes the descriptions of minerals identified up to that time, including two then unknown U minerals (designated "Unknown number 1" and "Unknown number 2"). Unknown number 2 has since been described as oswaldpeetersite and Unknown number 1 is described herein as the new mineral leesite.

PHYSICAL AND OPTICAL PROPERTIES

Leesite forms as aggregates of orange-yellow tablets up to 1 mm in diameter (Fig. 1). Tablets are flattened and stacked on {100}, the only well-developed crystal form (Fig. 2). Leesite also occurs as powdery masses in the interstices of gypsum crystals. Crystals are brittle with perfect cleavage on {100} and uneven fracture. No twinning was observed. Crystals are translucent with a vitreous luster, give a light yellow streak, and are non-fluorescent under LW and SW UV. The Mohs hardness is approximately 2, estimated by the behavior of crystals when broken. The density was not measured due to the limited availability of material. The calculated density is 3.256 g cm^{-3} based on the empirical formula. Leesite is readily soluble in dilute HCl and HNO_3, with no effervescence.

Leesite is optically biaxial (-), with $\alpha = 1.745(2)$, $\beta = 1.761(2)$, $\gamma = 1.765(2)$, (measured in white light). The $2V$ is 50(2)°, measured directly by conoscopic observation on a spindle stage; the calculated $2V$ is 52.7°. Dispersion is strong, $r > v$. The mineral is pleochroic with X nearly colourless, Y and Z orange yellow; $X < Y \approx Z$. The optical orientation is $X = \mathbf{a}$, $Y = \mathbf{c}$, $Z = \mathbf{b}$. The Gladstone-Dale compatibility, $1 - (K_p/K_c)$, is 0.037

(excellent) for the ideal formula, and 0.028 (excellent) for the empirical formula (Mandarino, 2007).

SPECTROSCOPY

Raman

The Raman spectrum of leesite was recorded using a Bruker Instruments Sentinel-785 laser head mounted on a Nikon Optiphot-2 microscope with Peltier-cooled CCD detector and integrated 785 nm diode laser, operated at 200 mW, with a spot size of 100 μm and ~5 cm^{-1} resolution (Fig. 3). The spectrum was acquired using a 10x objective, from 80 to 3200 cm^{-1} using five 3 s exposures, with five repeated acquisitions to improve the signal-to-noise ratio. The spectrometer was calibrated with software-controlled procedures (Opus software) using neon emission lines (wavelength calibration), and Tylenol® Raman bands (frequency calibration). A background correction was applied using the Opus software. In the Raman spectrum of leesite the ν_1 $(UO_2)^{2+}$ symmetric stretching vibration is present as a strong, complex band centered at 823 cm^{-1}. Splitting of ν_1 $(UO_2)^{2+}$ is concomitant with four unique U sites observed in the X-ray structure. Fitting reveals it is composed of four major bands, with centers at 840, 827, 818, and 802 cm^{-1}. Bartlett and Cooney (1989) provide an empirical relationship to derive the approximate U-O_{yl} bond lengths from the band positions assigned to the $(UO_2)^{2+}$ stretching vibrations, which gives 1.77 Å (840 cm^{-1}), 1.78 Å (827 cm^{-1}), 1.79 Å (818 cm^{-1}), and 1.81 Å (802 cm^{-1}). These values are in accordance with U–O_{yl} bond lengths given by Burns et al. (1997a) for the uranyl cation in pentagonal bipyramidal coordination, and from the X-ray data, however coincidence of ν_1 $(UO_2)^{2+}$ and δ-UOH (in-plane) bending modes is also possible in this

157 region. No bands were observed above 840 cm^{-1}, nor was there any evidence for ν_3
158 $(UO_2)^{2+}$ activated by symmetry distortion. A series of weak bands found in the 560-100
159 cm^{-1} region are attributed to various ν (U–O_{ligand}) stretches following the assignments
160 made by Dothée and Camelot (1982), Dothée et al. (1982), and Frost el al. (2007). Weak
161 bands at 557, 455, 435, and a very weak band at 398 cm^{-1} are assigned to ν_3 (U_3O) bridge
162 elongation modes. A weak band at 336 cm^{-1} is assigned to γ U_3O (out-of-plane bending),
163 and a weak band at 200 cm^{-1} to γ ($U_3(OH)_3$) out-of-plane bending vibrations. The
164 remaining bands near 160 and 120 cm^{-1} are assigned to $(UO_2)^{2+}$ translations and rotations.
165
166 **Infrared**
167 Attenuated total reflectance (ATR) Fourier transform infrared (FTIR) spectra were
168 obtained using a SENSIR Technologies IlluminatIR with a liquid N_2 cooled MCT detector
169 mounted to an Olympus BX51 microscope. An ATR objective was pressed into crystals of
170 leesite and the spectrum was measured from 4000 to 650 cm^{-1} (Fig. 4). The following band
171 assignments are based on those outlined by Čejka (1999). A broad, multicomponent
172 infrared band spanning from ~3500 to ~2400 cm^{-1} is related to the ν O–H stretching
173 vibrations of water molecules and hydroxyl groups (Fig. 5). The largest fitted band at 3000
174 cm^{-1} is attributed to the ν O–H stretching vibrations of hydrogen-bonded water molecules,
175 with a shoulder at 3450 cm^{-1} assigned to stretching vibrations of hydroxyl groups.
176 Comparison of the FWHM and area of these band suggest that the number of hydrogen-
177 bonding environments of hydroxyl groups is much less than the number of hydrogen-
178 bonding environments of the water molecules. Other fitted bands in this region are found at
179 3280, 2688, and 2522 cm^{-1}. Approximate O-H···O hydrogen bond-lengths calculated from
180 the observed stretching frequencies lie within the range ~2.9 to 2.6 Å using the correlation

function given by Libowitzky (1999). Several broad, low intensity bands between 2200-2000 cm^{-1} correspond to combination bands (δ H_2O and L H_2O). A weak band found at 1592 cm^{-1} is assigned as the ν_2 (δ)-bending vibration of hydrogen-bonded water. A very weak band appearing in the spectrum at 1420 cm^{-1} may be assigned to (SiO_3OH) modes from minor boltwoodite contamination, or to N-H bending vibrations of NH_4^+ molecules. The strong antisymmetric stretch ν_3 $(UO_2)^{2+}$ occurs at 920 cm^{-1}. The uranyl bond length inferred from the IR spectrum of leesite using the empirical relation given by Bartlett and Cooney (1989) is 1.77 Å. The ν_3 $(UO_2)^{2+}$ band is composed of a broad tail to higher wavenumber, and is formed by several overlapping δ-UOH (in-plane) bending modes with fitted centers at 1017, 995, 974, and 950 cm^{-1} (Fig. 4). No evidence of the (normally forbidden) ν_1 $(UO_2)^{2+}$ symmetric stretch was found. A remaining weak band centered at 764 cm^{-1} is attributed to γ UOH (out-of-plane bending) or H_2O libration modes.

CHEMICAL COMPOSITION

Electron microprobe analyses were deemed to be unreliable due to instability and decomposition of crystals under the electron beam. Instead, six chemical analyses were performed using Laser Ablation Inductively Coupled Plasma Mass Spectrometry (LA-ICP-MS). Six crystal aggregates were embedded in epoxy and polished to provide a flat surface (~50 x 50 μm). The ion signals for U, K, Pb, Na and Ca were measured using an Element 2 sector field high resolution inductively coupled plasma mass spectrometer (Thermo Fisher Scientific) in medium mass resolution mode coupled with a UP-213 (New Wave Research) Nd:YAG deep UV (213 nm) laser ablation system. Prior to the lasering of samples, the Element 2 was tuned using a multi-element solution containing 1 ng g^{-1} of each Li, In, and U to obtain maximum ion sensitivity. Laser ablation analyses involved acquiring

205 background ion signals for 60 seconds with the laser on and shuttered, and this was
206 followed by 60 seconds of data acquisition. Laser operating conditions involved using an 8
207 μm spot size, repetition rate of 5 Hz, 100% power out, which corresponded to a fluence of
208 ~8.4 J*cm^{-2}. Six areas on six crystals were examined using a raster scan, or single spot
209 analyses depending on the size of the crystals. Leesite contains appreciable U, K, Ca, some
210 Na, and negligible Pb, and the data are given in Table 2. No other elements were detected.
211 The ion signals (cps- counts per second) obtained for K, Ca, and Na are reported as a ratio
212 relative to that recorded for U, as absolute abundances could not be determined due to a
213 lack of an appropriate matrix matched external standard. The H_2O content was calculated
214 according to the structure on the basis of 20 O *apfu* with charge balance considerations.
215 The empirical formula, $K_{0.67}Na_{0.004}Ca_{0.012}U_4O_{20}H_{15.31}$, is calculated on the basis of 4 U and
216 20 O *apfu*. The ideal formula is $K(H_2O)_2[(UO_2)_4O_2(OH)_5]\cdot 3(H_2O)$, which requires: K_2O
217 3.55, UO_3 86.27, H_2O 10.18, total 100 wt%.
218

219 **POWDER X-RAY DIFFRACTION**

220 Powder diffraction data (Table 3) were obtained using a Rigaku R-Axis Rapid II
221 curved imaging plate microdiffractometer with monochromatized Mo*K*α radiation. A
222 Gandolfi-like motion on the φ and ω axes was used to randomize diffraction from the
223 sample. Observed *d*-values and intensities were derived by full profile fitting (Fig. S1,
224 Supplementary Information) using JADE 2010 software (Materials Data, Inc.). The unit-
225 cell parameters refined from the powder data using whole pattern fitting are a =
226 14.9163(16) Å, b = 14.1830(14) Å, c = 16.7336(18) Å, and V = 3540.1(6) Å^3.
227

228 **SINGLE CRYSTAL X-RAY DIFFRACTION AND REFINEMENT**

A homogenous plate fragment with sharp optical extinction in cross-polarized light was chosen for single-crystal X-ray diffraction study. Data were collected using Mo*K*α X-rays from a microfocus source and an Apex II CCD-based detector mounted to a Bruker Apex II Quazar three-circle diffractometer. Reflections were integrated and corrected for Lorentz, polarization, and background effects using the Bruker program SAINT. A multi-scan semi-empirical absorption correction was applied using equivalent reflections in SADABS-2012. An initial structure model was obtained by the intrinsic phasing method using SHELXT (Sheldrick, 2015) in space group *Pbca* with most atoms located, except some O atoms of water molecules. The SHELXL 2013 software package was used to refine the structure of leesite on the basis of F^2 for unique reflections, and the remaining O atoms of water were located in difference Fourier maps. Hydrogen atom positions were not determined, due to the weak X-ray scattering factor of hydrogen, and the dominance of U in the difference Fourier density maps. Furthermore, the diffraction pattern suffered from a split crystal contribution, with the heaviest contribution to low angle data. An attempt to deconvolute this contribution was made but did not improve the results. The split crystal, in combination with weak diffraction led to some difficulties during refinement of anisotropic displacement parameters for several oxygen atoms, and rigid bond restraints (RIGU) were applied to assists in their refinement. Details regarding the data collection and refinement results are given in the supplementary information and can also be found within the CIF, and bond-valence analysis is given in Table 4.

CRYSTAL STRUCTURE DESCRIPTION

Cation Coordination

The structure of leesite (Fig. 6) contains four symmetrically distinct U sites. All adopt [7]-fold pentagonal bipyramidal coordination, where the apices of each polyhedron are comprised of multiply bonded oxygen, forming the approximately linear uranyl ion—UO_2^{2+} (Burns et al., 1997a). Equatorially, each uranyl cation is five-coordinated by O or OH, and the polyhedra are linked by sharing edges arranged into the so-called fourmarierite anion sheet topology (Burns, 2005; Li and Burns, 2000; Lussier et al., 2016). The sheets in schoepite and metaschoepite also adopt the fourmarierite topology, which consists of sheets built from topological pentagons and triangles (Fig. 6). Pentagons are populated by U atoms, and triangles, arranged in alternating bow-tie arrangements, are vacant.

The interlayer of leesite is populated with K^+ cations and water molecules. Dimeric clusters of K^+ and H_2O serve to connect sheets of U polyhedra stacked along *a* by coordinating to their outstretched O_{yl} atoms (Fig. 7). Coordination about K^+ is [9]-fold and each K^+ binds six O_{yl} atoms and three water (Ow) molecules, such that the clusters have the composition $K_2O_{10}(H_2O)_4$. There is one symmetrically unique K site, and site-scattering refinement reveals it is partially occupied (0.71), in agreement with the average empirical chemistry (0.67 *apfu*). This is not unexpected, considering the analogous mineral fourmarierite also displays variable Pb^{2+} content (0.86 to 1.02 *apfu*) in natural and synthetic samples (Li and Burns, 2000). Atoms of Pb^{2+} in fourmarierite adopt a similar dimeric arrangement in the interlayer—with composition $Pb_2O_{10}(H_2O)_4$ (Fig. 6).

Relationship to other UOH minerals

The sheets of uranyl polyhedra in schoepite and metaschoepite are electroneutral, but can accommodate substitution of OH^- for O^{2-} within the sheet (Finch et al., 1996b).

This allows for variably charged sheets and the presence of interlayer cations. A synthetic Na-analog of metaschoepite is known, with an interlayer containing partially occupied Na^+ sites (Klingensmith et al., 2007). The arrangement of OH^- in leesite is identical to that found in the synthetic Na-analog of metaschoepite, and similar to metaschoepite in most regards except that a single OH^- group in metaschoepite is deprotonated in leesite (atom O9). Naturally occurring Na-rich metaschoepite is described by Sejkora et al. (2013) from the Jan Evangelista vein, Svornost mine in Jáchymov, and was shown to contain appreciable amounts of other elements (Na, 0.3 apfu; Cu, 0.13 apfu; Al, 0.13 apfu; Pb, 0.08 apfu). The Na-rich material is poorly crystalline and powdery, preventing its formal description as a mineral. Sejkora et al. (2013) also describe K-rich fourmarierite (0.2 to 0.45 K apfu) from the Evangelista vein, and recently, the schoepite family mineral kroupaite, $KPb_{0.5}[(UO_2)_8O_4(OH)_{10}](H_2O)_{10}$, has been described (Plášil et al., 2017). Structurally, kroupaite is similar to leesite, except K^+ cations adopt slightly different positions. Presumably, as Pb^{2+} content reaches ~50% in these phases, structural transformation to the fourmarierite cell is prompted by interlayer rearrangement and increased O^{2-} content within the sheets, however more work is required to understand the relationship between leesite, kroupaite, K-rich fourmarierite, and fourmarierite.

Foord et al. (1997) provide data for an unknown and incompletely characterized phase designated “mineral A” by Frondel (1956) that forms within “gummite” alteration rinds on uraninite from the Ruggles and Palermo granitic pegmatites in New Hampshire, USA. Powder diffraction analyses by Foord et al. (1997) indicate it is a mixture of schoepite-family minerals and other UOH phases. Composite chemical analyses by Foord et al. (1997) indicate the material contains appreciable K, Pb, and Ca; avg. (in wt%) UO_3 83.5, PbO 4.85, BaO 0.68, CaO 0.167, K_2O 2.46, SrO 0.21, ThO_2 0.85, H_2O 6.9, Σ99.62.

Given the similarity in chemical analyses to leesite, it appears that the mixture of schoepite-family minerals found in some "gummite" could contain leesite.

Bond valence analysis and role of interlayer H_2O

The symmetry of minerals in the schoepite family is sensitive to the water content, and presence of cations. Some relations between the cation content and arrangement of interlayer water are revealed by a bond-valence based approach, which examines interactions between the structural unit and the role of interstitial species (Hawthorne, 1992; Hawthorne and Schindler, 2008; Schindler and Hawthorne, 2004; Schindler and Hawthorne, 2008). The approach developed by these authors is a measure termed the charge-deficiency per anion (CDA), and is defined as the average bond-valence per O atom contributed by the interstitial species and adjacent structural units. Stable structures are formed when the bonding availability of the structural unit matches that of the interstitial complex (Hawthorne, 2012; Hawthorne, 2015). The quantity is useful for crystal-chemical predictions, enabling comparison between minerals with related topologies but differing interlayer constituents.

Bond valence analysis of the X-ray structure permits distinction of O atom types within the structure of leesite, and the ideal structural formula assuming full K^+ occupancy is $K(H_2O)_2[(UO_2)_4O_2(OH)_5]\cdot 3(H_2O)$. The CDA of the sheet in leesite is 0.133, identical to the value for Na-metaschoepite. The value is intermediate to those of schoepite and metaschoepite (0.08) and fourmarierite (0.19). The range in Lewis basicity of the structural unit in leesite is 0.13-0.24 using the method of Schindler and Hawthorne (2008), and is comparable to ranges calculated for other uranyl-oxide hydroxyl-hydrate minerals (e.g. schoepite: 0.11-0.20).

When present in the interstitial complex, (H_2O) molecules act as transformers of bond-valence from cations within the interlayer to atoms in the structural unit (Schindler and Hawthorne 2008). The interlayer of leesite contains 5 unique (H_2O) molecules. The atoms Ow1, Ow2, Ow3, and Ow4 are [5]-coordinated and transfer weak bond valence from K^+ to uranyl ion oxygen atoms within the sheet through various interactions, and according to the designation given by Schindler and Hawthorne (2008), are considered inverse-transformer (H_2O) groups. Atom Ow1 forms two bonds to K^+, two weak H-bonds with uranyl ions of the sheet (~0.2 *vu*), and one H-bond with Ow2. Atoms Ow2, Ow3, and Ow4 each link to two H atoms (2 x 0.8 *vu*) of other (H_2O) molecules, and all form at least one H-bond to uranyl ions of the sheet. They also each accept one H-bond (0.2 *vu*) from (OH) groups of the sheet. The remaining (H_2O) group, Ow5, does not bond to a cation and has coordination number [4]. Thus, Ow5 acts as a non-transformer group by propagating weak bond valence from cations to anions that are too distant to bond directly to the cation. Details regarding the number of H-bonds donated and accepted, and their interatomic (O-H···O) distances are given in Table 4 and Table S3 (Supplementary Information), respectively.

It is difficult to establish if hydronium (H_3O^+) is present in schoepite family phases with non-stoichiometric cation contents (Wilkins and Mateen, 1974), but this would be in accord with the observation that leesite and other members of the family are formed from acidic solutions. Site scattering refinement indicates slightly higher K^+ occupancy (0.71) than obtained from LA-ICP-MS analyses (0.67 *apfu*), which suggests the presence of disordered O (H_3O^+) or N (NH_4^+) atoms at this site, instead of vacancies. However, the discrepancy in refined occupancy may be related to an inadequate absorption correction. It is currently unclear if partial K^+ occupancy is accounted for by $OH^- \Leftrightarrow O^{2-}$ substitution in

348 the sheet, or through interlayer NH_4^+ or H_3O^+ substitution, but due to their similar sizes,
349 H_3O^+ and NH_4^+ could readily substitute for K^+ in leesite.
350
351 **Speciation of interlayer cations**
352 With details of the range of bonding availability of the structural unit and interlayer
353 (H_2O), we now have the necessary information to describe the species of cations that can
354 be expected to occur in the interlayer in schoepite family minerals as demonstrated by
355 Schindler and Hawthorne (2004) and Schindler and Hawthorne (2008). Figure 8 depicts
356 the variation in Lewis acidity for various cation coordination numbers and charges with
357 differing numbers of coordinating transformer (H_2O) groups. A stable structure is formed
358 where lines of variable Lewis acidity overlap the Lewis basicity range of the structural unit
359 (shown in blue). As revealed in Figure 8, cations with coordination number >[8] must bond
360 to at least one inverse-transformer (H_2O) group to produce a stable structure (Schindler and
361 Hawthorne, 2008). In the structure of leesite, potassium cations are coordinated by three
362 inverse-transformer (H_2O) groups (2 x Ow1, and Ow3), and this agrees with the predicted
363 coordination number of 0 transformer (H_2O) groups.
364 Monovalent cations with a wide range of coordination numbers can be incorporated
365 into the interlayer of leesite, and may include H_3O^+, NH_4^+, Na^+, or Cs^+. Incorporation of
366 [8]-coordinate Ca^{2+} is possible; however, others have documented conversion of
367 metaschoepite to becquerelite in the presence of Ca^{2+} at elevated temperatures (Sandino
368 and Grambow, 1994; Sowder et al., 1996; Sowder et al., 1999). Although leesite occurs
369 intimately with gypsum, it contains relatively little Ca^{2+} (Table 1). Ca-rich metaschoepite
370 may be more likely to occur in carbonate-rich assemblages, such as those at the Markey
371 mine to the nearby southwest. Hydrolysis reactions with abundant uranyl carbonates found

372 there may lead to the formation of Na, or Ca-metaschoepite. Samples of Na-rich
373 metaschoepite from Jáchymov were shown to contain small amounts of Cu^{2+} and Al^{3+}, and
374 we can expect these cations will occupy sites that maximize coordination by transformer
375 (H_2O) groups (Sejkora et al., 2013).
376

377 **RENEWED INTEREST IN PARASCHOEPITE?**

378 In a dry environment, schoepite slowly loses interlayer water (Kubatko et al., 2006;
379 O'Hare et al., 1988), leading to a decrease in the interplanar spacing between sheets as
380 water molecules rearrange and relocate, forming a new H-bonded array in metaschoepite
381 (Weller et al., 2000). Schoep and Stradiot (1947) noted an opaque lemon yellow
382 orthorhombic phase within altered crystals of schoepite, which was indistinguishable from
383 crystals of schoepite except upon determination of its optical properties. A combination of
384 optical and chemical analyses indicated the material is unique from other schoepite family
385 members, with the formula $UO_3 \cdot 1.9H_2O$, and was thus designated paraschoepite. Christ
386 and Clark (1960) report a large interplanar distance (c = 15.22 Å) for single crystals of
387 paraschoepite, and state "Because of the distinctive X-ray pattern given by the yellow
388 crystals and the excellent agreement of the optical measurements obtained in the present
389 study with those originally given by Schoep and Stradiot in 1947, there can be little doubt
390 as to the validity of paraschoepite." Subsequent descriptions have attributed paraschoepite
391 to a mixture of metaschoepite, dehydrated schoepite, and ianthinite (Brugger et al., 2011;
392 Finch et al., 1997; Finch et al., 1992); however, the similar large interplanar spacing (a
393 =14.87 Å) and arrangements found in leesite may be in part related to paraschoepite.
394 Leesite contains a predominance of inverse-transformer (H_2O) groups, which maximize
395 interactions with the sheet in the presence of bulky K^+ cations. In paraschoepite, interlayer

396 water remaining after partial dehydration would likely rearrange in order to maximize
397 bonding interactions with the sheet. This is best achieved by the inclusion of more inverse-
398 transformer (H_2O) group interactions, which are capable of transferring bond strength at
399 longer distances. Finch et al. (1992) argue that paraschoepite represents a metastable
400 structure where localized expansion is associated with the collapse of layers as "dehydrated
401 schoepite" forms. Local expansion of layers may be related to reorganization of interlayer
402 (H_2O) groups from transformer to inverse-transformer roles, and future X-ray or neutron
403 studies exploring this metastable state may be supplemented by our observations of the
404 structure of leesite.
405

406 **IMPLICATIONS**

407 With the description of leesite, we are better able to recognize the conditions and
408 crystal-chemical features that drive formation of specific minerals in the schoepite family.
409 Details of the cation arrangement, water content and H-bonding array can be compared for
410 this series of minerals, and predictions can be made towards possible compositions not yet
411 observed. Our observations of natural samples from several localities reveal that the
412 fourmarierite sheet anion topology is capable of accommodating an interlayer with a range
413 of heterovalent cations and unique configurations. Recognizing how and where large K^+
414 cations incorporate into this family reveals how short-lived radionuclides like ^{137}Cs or ^{90}Sr
415 will behave during the initial alteration stages of irradiated nuclear fuel (Giammar and
416 Hering, 2004). Long-lived radionuclides, such as ^{135}Cs or ^{237}Np, may also be incorporated,
417 albeit under different circumstances. Low-valence cations (Cs^+ and Sr^{2+}) will accumulate
418 within interlayer space during formation, or through cation exchange within the interlayer.
419 The incorporation mechanism for high-valence cations (e.g. $Np^{5+,6+}$, $Pu^{5+,6+}$) depends

heavily on the oxidation state, and whether the structure can support substitution of actinyl ions $(An^{5+,6+}O_2)^{1+,2+}$ for uranyl ions $(UO_2)^{2+}$ within the sheet of polyhedra (Burns et al., 1997b). Incorporation of $(Np^{5+}O_2)^{+}$ must be accompanied by an appropriate charge-balancing mechanism; through protonation of the sheet, or inclusion of cations (Burns et al., 2004; Klingensmith et al., 2007). Schoepite family phases formed during the initial alteration stages will readily incorporate the elements listed above through these processes, but may be subsequently altered, or undergo structural rearrangement. For example, Sandino and Grambow (1994) observed the complete conversion of metaschoepite into compreignacite in the presence of excess K^{+} at room temperature. Leesite from the Jomac mine is intimately associated with compreignacite, and facile conversion to compreignacite may explain the rarity of leesite. In this case, the crystal-chemical predictability afforded by the bond-valence approach is very powerful due to the penchant for UOH minerals to form, rearrange and redistribute U or cations (Finch et al., 1992).

ACKNOWLEDGEMENTS

This research is funded by the Office of Basic Energy Sciences of the U.S. Department of Energy as part of the Materials Science of Actinides Energy Frontier Research Center (DE-SC0001089). The Element2 HR-ICP-MS instrument used for chemical analyses is housed within the Midwest Isotope and Trace Element Research Analytical Center (MITERAC) at the University of Notre Dame. Electron microscopy was carried out in the Applied Chemical and Morphological Analysis Laboratory at Michigan Technological University. The John Jago Trelawney Endowment to the Mineral Sciences Department of the Natural History Museum of Los Angeles County funded a portion of this study. Jakub Plášil is thankful for the support from the project GACR 15-12653S

444
445
446 **RFERENCES CITED**
447
448 Amonette, J.E., Holdren, G.R., Jr., Krupa, K.M., and Lindenmeier, C.W. (1994) Assessing
449 the Environmental Availability of Uranium in Soils and Sediments. NUREG/CR-
450 6232 PNL-9570, Pacific Northwest Laboratory, Richland, WA.
451 URL:http://www.iaea.org/inis/collection/NCLCollectionStore/_Public/25/069/2506
452 9667.pdf?r=1. Accessed: 2017-08-13. (Archived by WebCite® at
453 http://www.webcitation.org/6shXVIKZO)
454 Bartlett, J.R., and Cooney, R.P. (1989) On the determination of uranium-oxygen bond
455 lengths in dioxouranium(VI) compounds by Raman spectroscopy. Journal of
456 Molecular Structure, 193, 295-300.
457 Brugger, J., Meisser, N., Etschmann, B., Ansermet, S., and Pring, A. (2011)
458 Paulscherrerite from the Number 2 Workings, Mount Painter Inlier, Northern
459 Flinders Ranges, South Australia: "Dehydrated schoepite" is a mineral after all.
460 American Mineralogist, 96(2-3), 229-240.
461 Burns, P.C. (2005) U^{6+} minerals and inorganic compounds: Insights into an expanded
462 structural hierarchy of crystal structures. The Canadian Mineralogist, 43(6), 1839-
463 1894.
464 Burns, P.C., Deely, K.M., and Skanthakumar, S. (2004) Neptunium incorporation into
465 uranyl compounds that form as alteration products of spent nuclear fuel:
466 Implications for geologic repository performance. Radiochimica Acta, 92(3), 151-
467 159.
468 Burns, P.C., Ewing, R.C., and Hawthorne, F.C. (1997a) The crystal chemistry of
469 hexavalent uranium; polyhedron geometries, bond-valence parameters, and
470 polymerization of polyhedra. The Canadian Mineralogist, 35(6), 1551-1570.
471 Burns, P.C., Ewing, R.C., and Miller, M.L. (1997b) Incorporation mechanisms of actinide
472 elements into the structures of U^{6+} phases formed during the oxidation of spent
473 nuclear fuel. Journal of Nuclear Materials, 245(1), 1-9.
474 Čejka, J. (1999) Infrared spectroscopy and thermal analysis of the uranyl minerals. In P.C.
475 Burns, and R.C. Ewing, Eds. Uranium: Mineralogy, Geochemistry and the
476 Environment, 38, p. 521-622. Mineralogical Society of America.
477 Christ, C.L., and Clark, J.R. (1960) Crystal chemical studies of some uranyl oxide
478 hydrates. American Mineralogist, 45(9-10), 1026-1061.
479 Dothée, D.G., and Camelot, M.M. (1982) Vibrational Spectroscopy of potassium
480 hexauranate hydrate. I. Frequencies assignable to oxygen-atoms motions -
481 hypothesis on the structure of the anionic layer. Bulletin de la Société chimique de
482 France, (3-4), 97-102.
483 Dothée, D.G., Fahys, B.R., and Camelot, M.M. (1982) Vibrational spectroscopy of
484 potassium hexauranate hydrate. II. Motions of hygrogen atoms - hypothesis on the
485 water-structure in the uranate. Bulletin de la Société chimique de France, (3-4),
486 103-108.
487 Finch, K.J., Suksi, J., Rasilainen, K., and Ewing, R.C. (1996a) Uranium-series ages of
488 secondary uranium minerals with applications to the long-term evolution of spent
489 nuclear fuel. In W.M. Murphy, and D.A. Knecht, Eds. Scientific Basis for Nuclear
490 Waste Management Xix, 412, p. 823-830. Materials Research Society, Pittsburgh.

Finch, R.J., Cooper, M.A., Hawthorne, F.C., and Ewing, R.C. (1996b) The crystal structure of schoepite, $[(UO_2)_8O_2(OH)_{12}](H_2O)_{12}$. The Canadian Mineralogist, 34, 1071-1088.

Finch, R.J., and Ewing, R.C. (1992) The corrosion of uraninite under oxidizing conditions. Journal of Nuclear Materials, 190, 133-156.

Finch, R.J., Hawthorne, F.C., Miller, M.L., and Ewing, R.C. (1997) Distinguishing among schoepite, $[(UO_2)_8O_2(OH)_{12}](H_2O)_{12}$, and related minerals by X-ray powder diffraction. Powder Diffraction, 12(4), 230-238.

Finch, R.J., Miller, M.L., and Ewing, R.C. (1992) Weathering of natural uranyl oxide hydrates - schoepite polytypes and dehydration effects. Radiochimica Acta, 58-9, 433-443.

Finch, R.J., and Murakami, T. (1999) Systematics and paragenesis of uranium minerals. In P.C. Burns, and R.C. Ewing, Eds. Uranium: Mineralogy, Geochemistry and the Environment, 38, p. 91-179. Mineralogical Society of America.

Foord, E.E., Korzeb, S.L., Lichte, F.E., and Fitzpatrick, J.J. (1997) Additional studies on mixed uranyl oxide-hydroxide hydrate alteration products of uraninite from the Palermo and Ruggles granitic pegmatites, Grafton County, New Hampshire. The Canadian Mineralogist, 35, 145-151.

Frondel, C. (1956) Mineral compostion of gummite. American Mineralogist, 41(7-8), 539-568.

Frost, R. L., Čejka, J., & Weier, M. L. (2007). Raman spectroscopic study of the uranyl oxyhydroxide hydrates: becquerelite, billietite, curite, schoepite and vandendriesscheite. Journal of Raman Spectroscopy, 38, 460-466.

Giammar, D.E., and Hering, J.G. (2004) Influence of dissolved sodium and cesium on uranyl oxide hydrate solubility. Environmental Science & Technology, 38(1), 171-179.

Hawthorne, F.C. (1992) The role of OH and H_2O in oxide and oxysalt minerals. Zeitschrift für Kristallographie, 201(3-4), 183-206.

-. (2012) A bond-topological approach to theoretical mineralogy: crystal structure, chemical composition and chemical reactions. Physics and Chemistry of Minerals, 39(10), 841-874.

-. (2015) Toward theoretical mineralogy: A bond-topological approach. American Mineralogist, 100(4), 696-713.

Hawthorne, F.C., and Schindler, M. (2008) Understanding the weakly bonded constituents in oxysalt minerals. Zeitschrift für Kristallographie - Crystalline Materials, 223, p. 41.

Haynes, P.E. (2000) Mineralogy of the Jomac Mine, San Juan county, Utah. Rocks and Minerals, 75(4), 240-248.

Klingensmith, A.L., Deely, K.M., Kinman, W.S., Kelly, V., and Burns, P.C. (2007) Neptunium incorporation in sodium-substituted metaschoepite. American Mineralogist, 92(4), 662-669.

Kubatko, K.A., Helean, K., Navrotsky, A., and Burns, P.C. (2006) Thermodynamics of uranyl minerals: Enthalpies of formation of uranyl oxide hydrates. American Mineralogist, 91(4), 658-666.

Li, Y., and Burns, P.C. (2000) Investigations of crystal-chemical variability in lead uranyl oxide hydrates. II. Fourmarierite. The Canadian Mineralogist, 38(3), 737-749.

Libowitzky, E. (1999) Correlation of O-H stretching frequencies and O-H···O hydrogen bond lengths in minerals. Monatshefte Für Chemie, 130(8), 1047-1059.

Lussier, A.J., Burns, P.C., and King-Lopez, R. (2016) A revised and expanded structure hierarchy of natural and synthetic hexavalent uranium compounds. The Canadian Mineralogist, 54(1), 177-283.

Mandarino, J.A. (2007) The Gladstone-Dale compatibility of minerals and its use in selecting mineral species for further study. The Canadian Mineralogist, 45, 1307-1324.

O'Hare, P.A.G., Lewis, B.M., and Nguyen, S.N. (1988) Thermochemistry of uranium compounds XVII. Standard molar enthalpy of formation at 198.15 K of dehydrated schoepite $UO_3 \cdot 0.9\ H_2O$. Thermodynamics of (schoepite + dehydrated schoepite + water). Journal of Chemical Thermodynamics, 20(11), 1287-1296.

Plášil, J. (2014) Oxidation-hydration weathering of uraninite: the current state-of-knowledge. Journal of Geosciences, 59(2), 99-114.

Plášil, J., Škoda, R., Čejka, J., Bourgoin, V., and Boulliard, J.-C. (2016) Crystal structure of the uranyl-oxide mineral rameauite. European Journal of Mineralogy, 28, 959-967.

Plášil, J., Kampf, A.R., Olds, T.A., Sejkora, J., Škoda, R., Burns, P.C., and Čejka, J. (2017) Kroupaite, IMA 2017-031. CNMNC Newsletter No. 38, Aug 2016; Mineralogical Magazine, **81(4)**, 1033-1038.

Sandino, M.C.A., and Grambow, B. (1994) Solubility equilibria in the U(VI)-Ca-K-Cl-H_2O system: transformation of schoepite into becquerelite and compreignacite. Radiochimica Acta, 66-7, 37-43.

Schindler, M., and Hawthorne, F.C. (2004) A bond-valence approach to the uranyl-oxide hydroxy-hydrate minerals: Chemical composition and occurrence. The Canadian Mineralogist, 42(6), 1601-1627.

-. (2008) The stereochemistry and chemical compostion of interstitial complexes in uranyl-oxysalt minerals. The Canadian Mineralogist, 46(2), 467-501.

Schoep, A., and Stradiot, S. (1947) Paraschoepite and epiianthinite, two new uranium minerals from Shinkolobwe (Belgian Congo). American Mineralogist, 32(5-6), 344-350.

Sejkora, J., Plášil, J., and Bureš, B. (2013) Unusual assocation of supergene uranium minerals from the Jan Evangelista vein, Jáchymov (Czech Republic). Bulletin mineralogicko-petrologického oddělení Národního Muzea (Praha), 21, 143-156.

Sheldrick, G.M. (2015) SHELXT - Integrated space-group and crystal-structure determination. Acta Crystallographica A-Foundation and Advances, 71, 3-8.

Sowder, A.G., Clark, S.B., and Fjeld, R.A. (1996) The effect of silica and phosphate on the transformation of schoepite to becquerelite and other uranyl phases. Radiochimica Acta, 74, 45-49.

Sowder, A.G., Clark, S.B., and Field, R.A. (1999) The transformation of uranyl oxide hydrates: The effect of dehydration on synthetic metaschoepite and its alteration to becquerelite. Environmental Science & Technology, 33(20), 3552-3557.

Taylor, J.C., and Hurst, H.J. (1971) The hydrogen-atom locations in the [alpha] and [beta] forms of uranyl hydroxide. Acta Crystallographica Section B, 27(10), 2018-2022.

Trites, A.F., Jr., and Hadd, G.A. (1958) Geology of the Jomac Mine, White canyon area, San Juan county, Utah. U.S. Geological Survey Bulletin, 1046-H.

Vochten, R., and Deliens, M. (1998) Blatonite, $UO_2CO_3 \cdot H_2O$, a new uranyl carbonate monohydrate from San Juan County, Utah. The Canadian Mineralogist, 36, 1077-1081.

Vochten, R., Deliens, M., and Medenbach, O. (2001) Oswaldpeetersite, $(UO_2)_2CO_3(OH)_2(H_2O)_4$, a new basic uranyl carbonate mineral from the Jomac uranium mine, San Juan County, Utah, USA. The Canadian Mineralogist, 39, 1685-1689.

Walenta, K., and Theye, T. (2012) Heisenbergite, a new uranium mineral from the uranium deposit of Menzenschwand in the Southern Black Forest, Germany. Neues Jahrbuch für Mineralogie, 189(2), 117-123.

Walker, T.L. (1923) Schoepite, a new uranium mineral from Kasolo, Belgian Congo. American Mineralogist, 8(4), 67-69.

Weller, M.T., Light, M.E., and Gelbrich, T. (2000) Structure of uranium(VI) oxide dihydrate, $UO_3 \cdot 2H_2O$; synthetic meta-schoepite $(UO_2)_4O(OH)_6 \cdot 5H_2O$. Acta Crystallographica Section B-Structural Science, 56, 577-583.

Wilkins, R.W.T., and Mateen, A. (1974) The spectroscopic study of oxonium ions in minerals. American Mineralogist, 59, 811-819.

Wood, R.M., and Palenik, G.J. (1999) Bond valence sums in coordination chemistry using new R_0 values. Potassium−oxygen complexes. Inorganic Chemistry, 38(5), 1031-1034.

Wronkiewicz, D.J., Bates, J.K., Gerding, T.J., Veleckis, E., and Tani, B.S. (1992) Uranium release and secondary phase formation during unsaturated testing of UO_2 at 90°C. Journal of Nuclear Materials, 190, 107-127.

FIGURE CAPTIONS

Figure 1. Orange-yellow aggregates of leesite rim the edges of blocky orange compreignacite, with pale yellow sklodowskite. The whole assemblage sits atop colorless gypsum, with probable white nickelalumite or mbobomkulite. Horizontal field of view is 2 mm.

Figure 2. Secondary electron image of tabular leesite stacked along (100). Photo by Shawn M. Carlson and Owen P. Mills.

Figure 3. Raman spectrum of leesite in the 1600 to 100 cm^{-1} range, taken with a 785 nm laser. (Inset) Fitted bands for ν_1 $(UO_2)^{2+}$, in the region from 870 to 780 cm^{-1}.

Figure 4. Infrared spectrum (ATR) of leesite from 4000 to 600 cm^{-1}. (Inset) Fitted bands for ν_3 $(UO_2)^{2+}$ in the 1040 to 880 cm^{-1} region.

Figure 5. Fitted bands for ν O-H in the 4000 to 2200 cm^{-1} infrared region.

Figure 6. A comparative view of the anion sheet topologies, $(OH)^-$ distributions, and cation positions for analogous uranyl-oxide hydroxy-hydrates. Black circles highlight vertices containing $(OH)^-$, and bare vertices represent O^{2-}. The distribution of $(OH)^-$ in leesite is identical to that of the synthetic Na-analog of metaschoepite. Potassium (blue), lead (orange), sodium (yellow).

Figure 7. A polyhedral representation of the uranyl oxide hydroxide sheet (yellow) in leesite, with ball-and-stick interlayer containing water oxygen (red) and potassium (blue).

Figure 8. The variation in Lewis acidity for particular cation coordination numbers and charges of a general interstitial complex with differing numbers of transformer (H_2O) groups. The range in Lewis basicity of the structural unit of leesite is shown in blue. A stable structure is formed where the lines of variable Lewis acidity overlap the Lewis basicity of the structural unit. Figure adapted in part from Schindler and Hawthorne (2004).

This is a preprint, the final version is subject to change, of the American Mineralogist (MSA)
Cite as Authors (Year) Title. American Mineralogist, in press.
DOI: http://dx.doi.org/10.2138/am-2018-6083

Figure 1

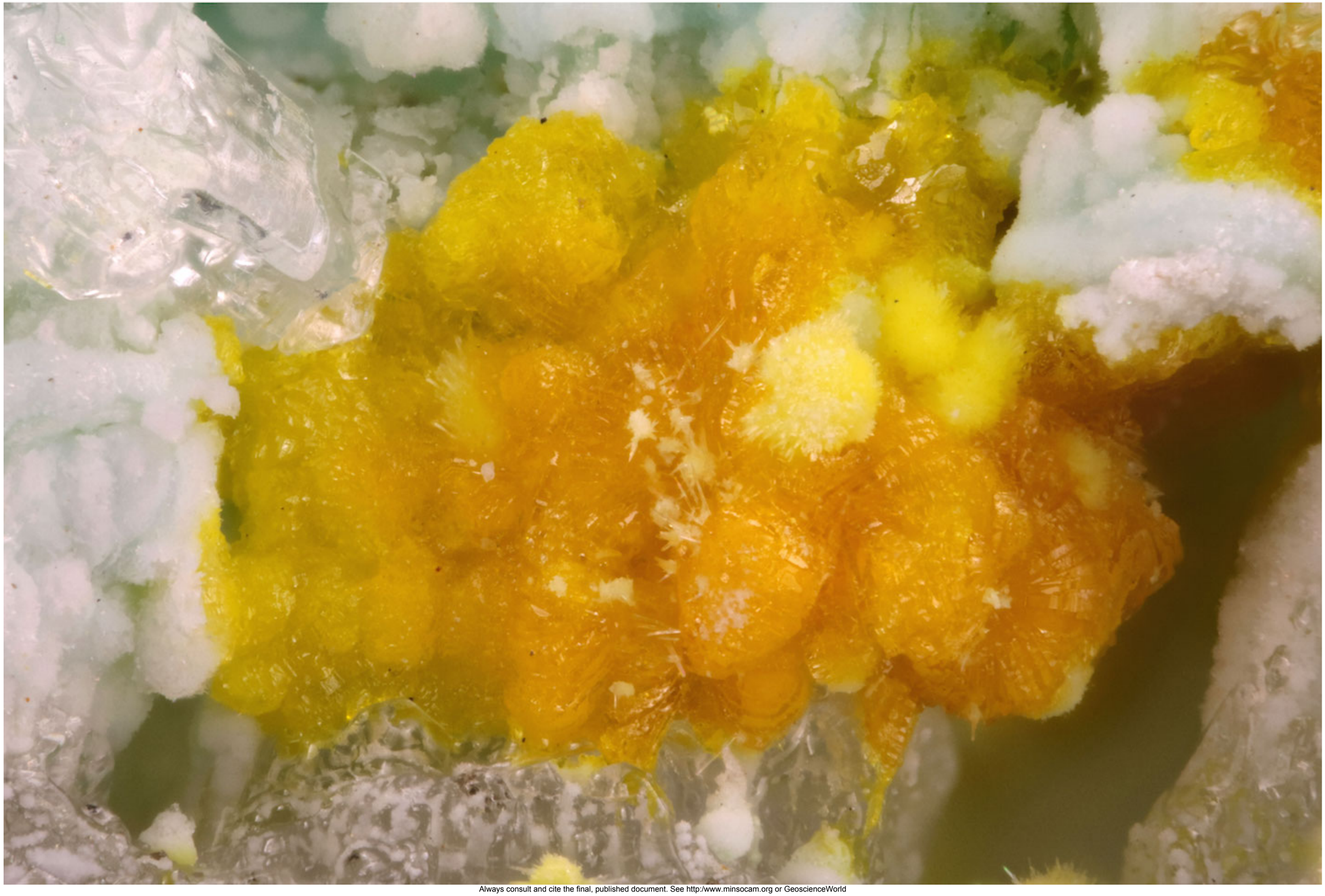

This is a preprint, the final version is subject to change, of the American Mineralogist (MSA)
Cite as Authors (Year) Title. American Mineralogist, in press.
DOI: http://dx.doi.org/10.2138/am-2018-6083

Figure 2

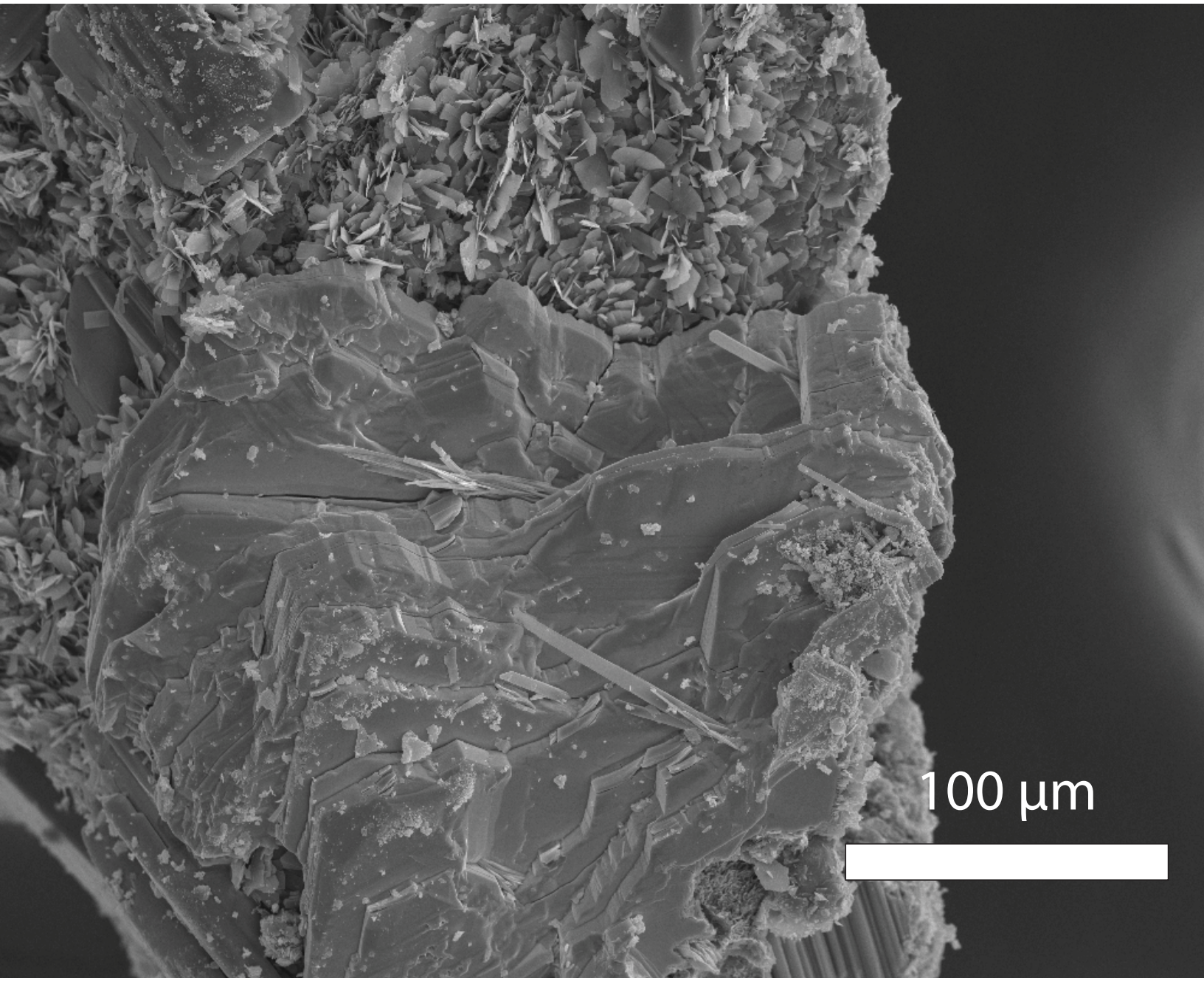

This is a preprint, the final version is subject to change, of the American Mineralogist (MSA)
Cite as Authors (Year) Title. American Mineralogist, in press.
DOI: http://dx.doi.org/10.2138/am-2018-6083

Figure 3

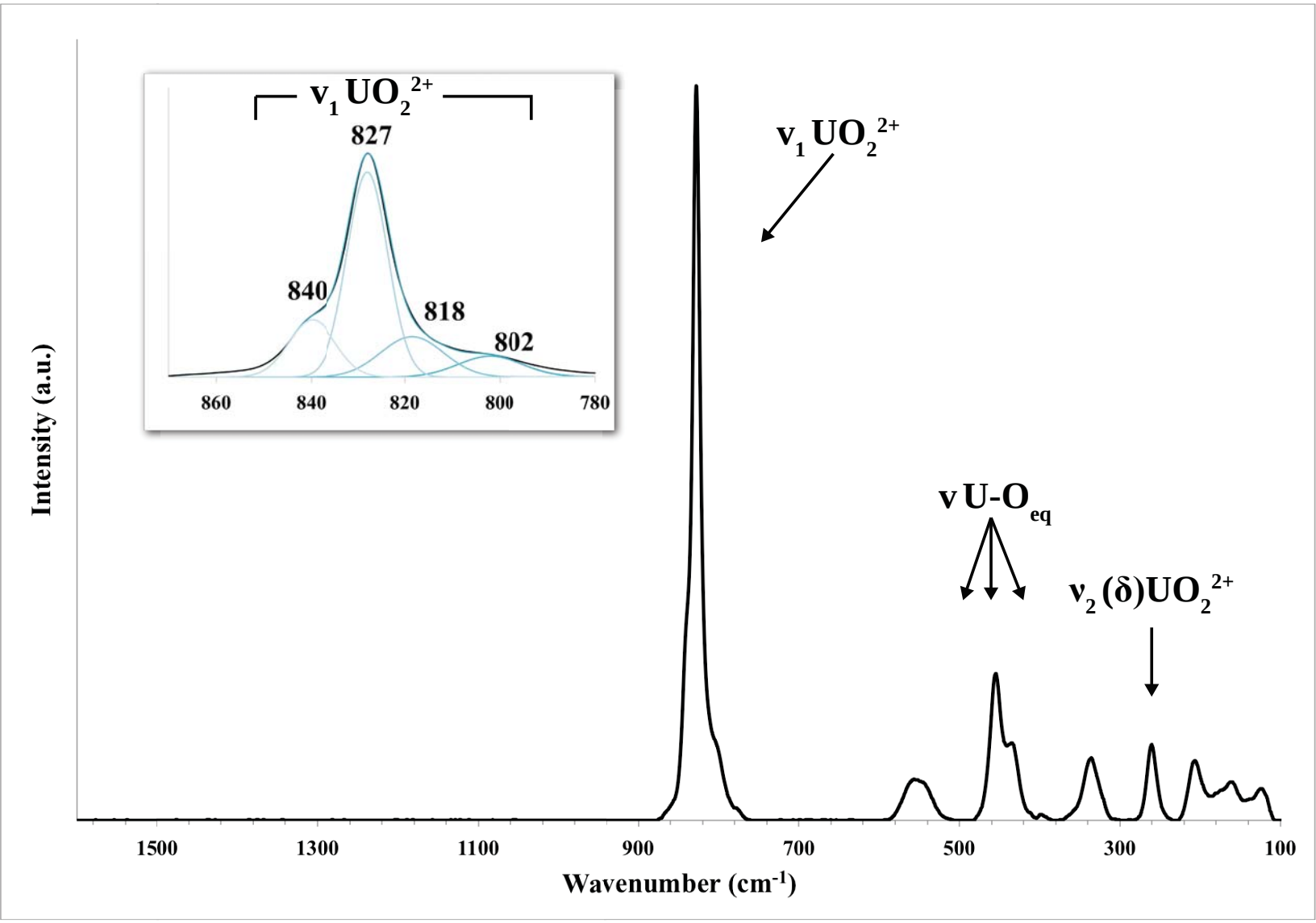

This is a preprint, the final version is subject to change, of the American Mineralogist (MSA)
Cite as Authors (Year) Title. American Mineralogist, in press.
DOI: http://dx.doi.org/10.2138/am-2018-6083

Figure 4

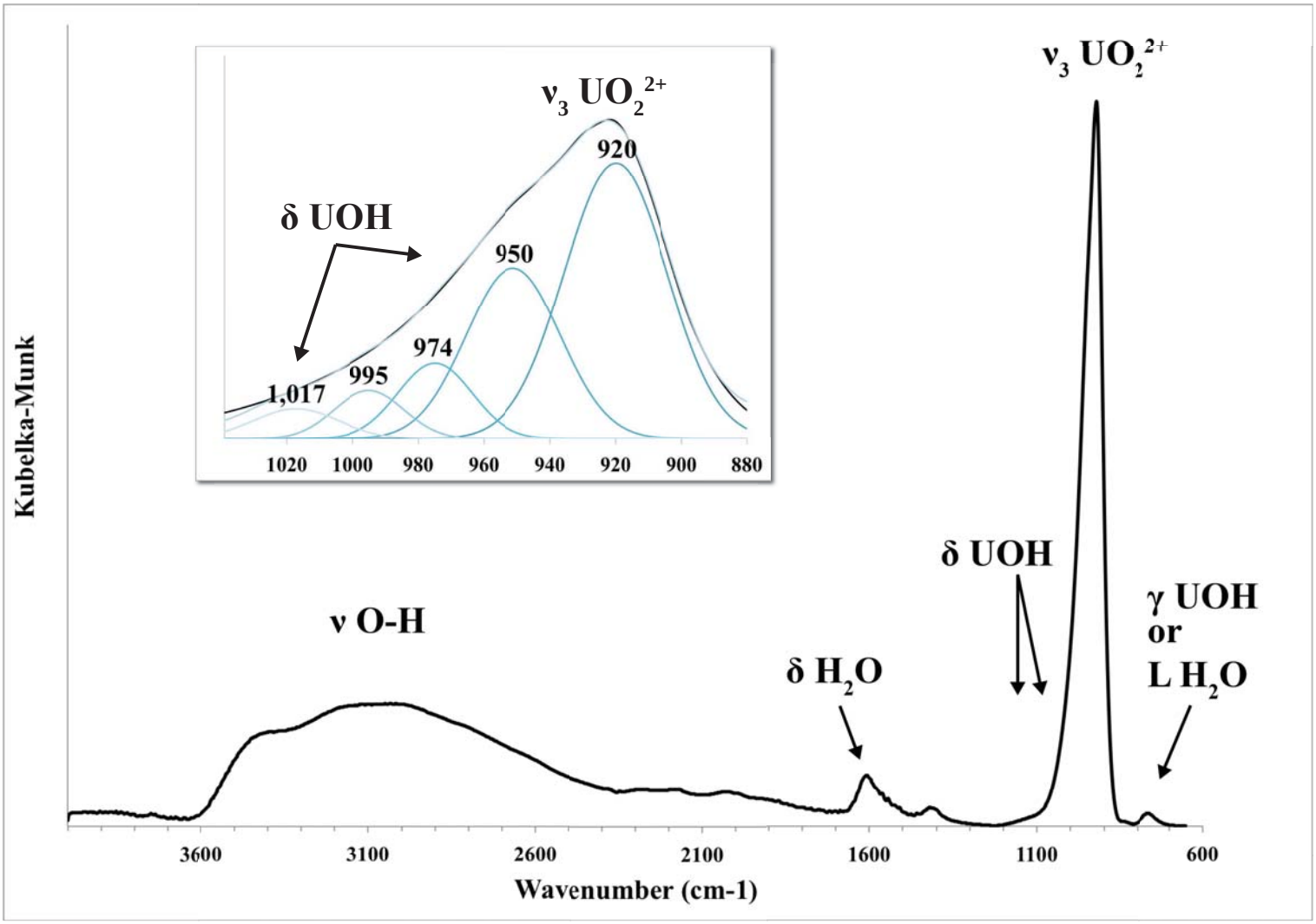

This is a preprint, the final version is subject to change, of the American Mineralogist (MSA)
Cite as Authors (Year) Title. American Mineralogist, in press.
DOI: http://dx.doi.org/10.2138/am-2018-6083

Figure 5

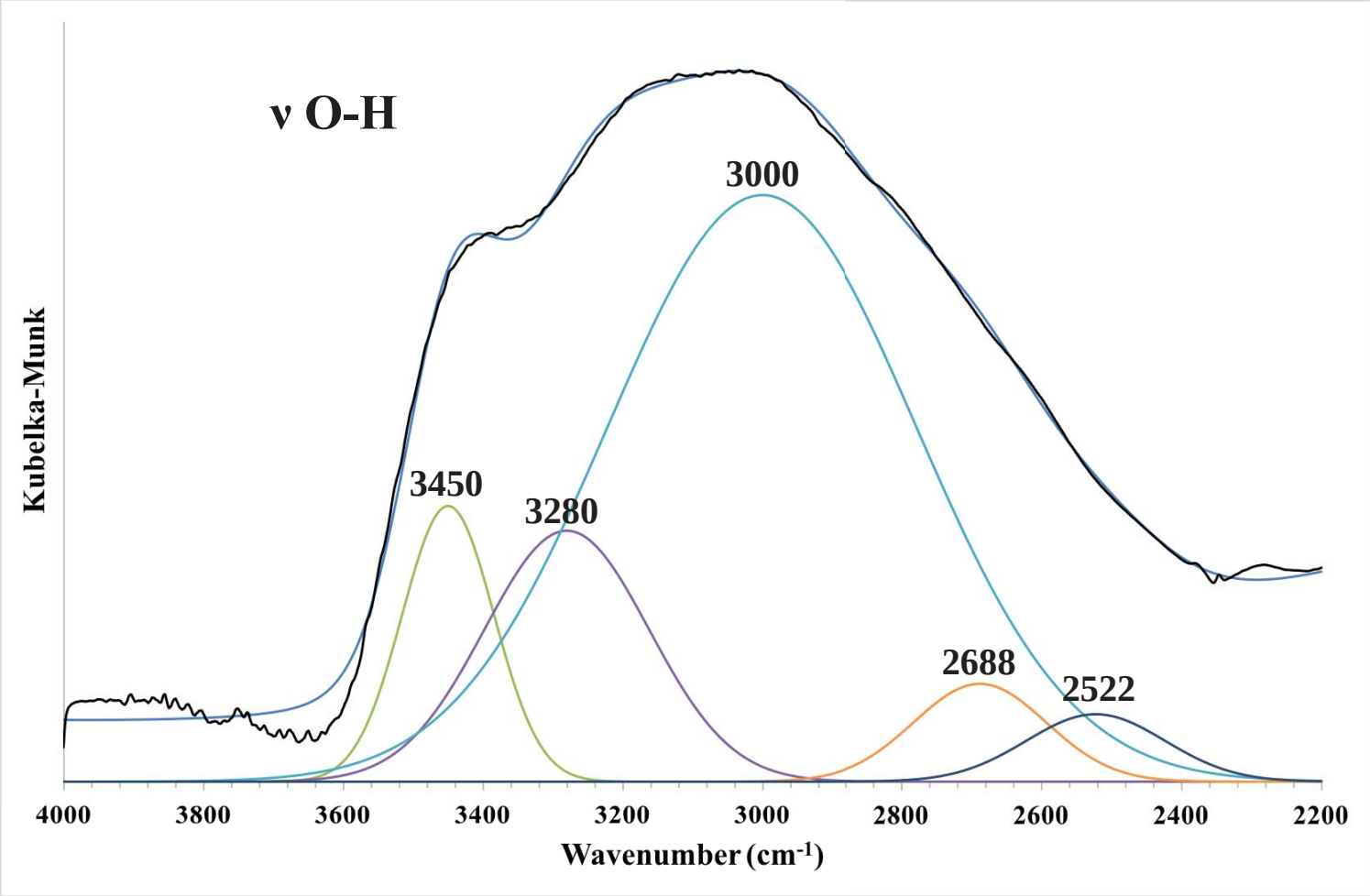

This is a preprint, the final version is subject to change, of the American Mineralogist (MSA)
Cite as Authors (Year) Title. American Mineralogist, in press.
DOI: http://dx.doi.org/10.2138/am-2018-6083

Figure 6

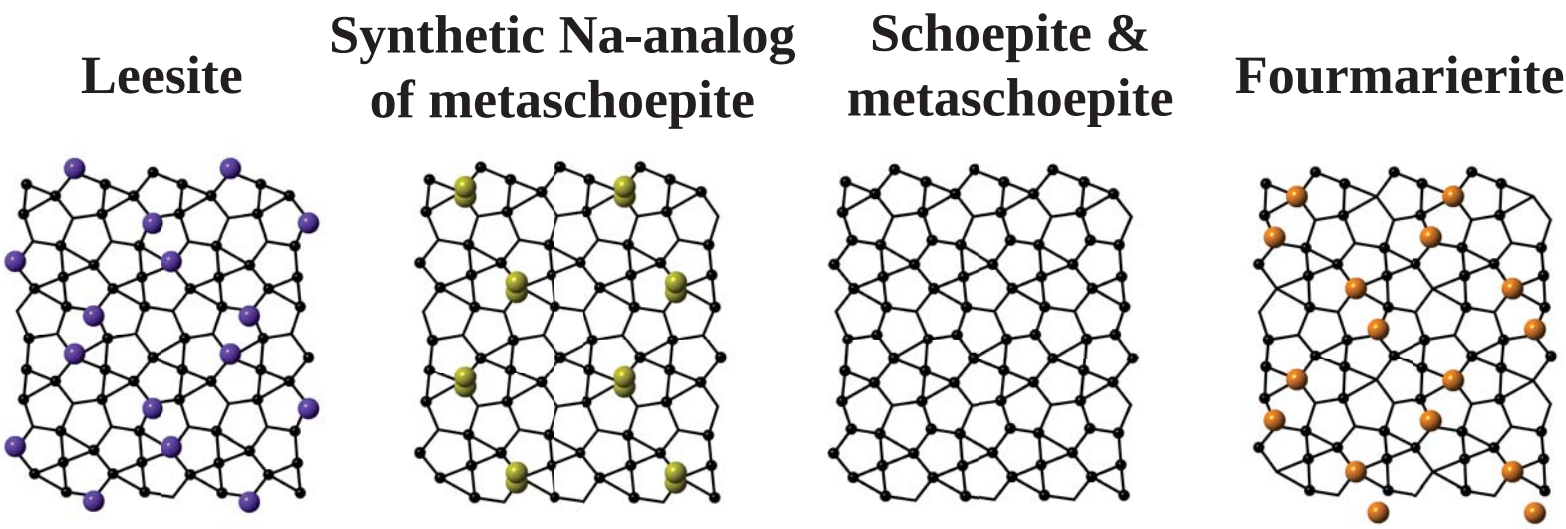

This is a preprint, the final version is subject to change, of the American Mineralogist (MSA)
Cite as Authors (Year) Title. American Mineralogist, in press.
DOI: http://dx.doi.org/10.2138/am-2018-6083

Figure 7

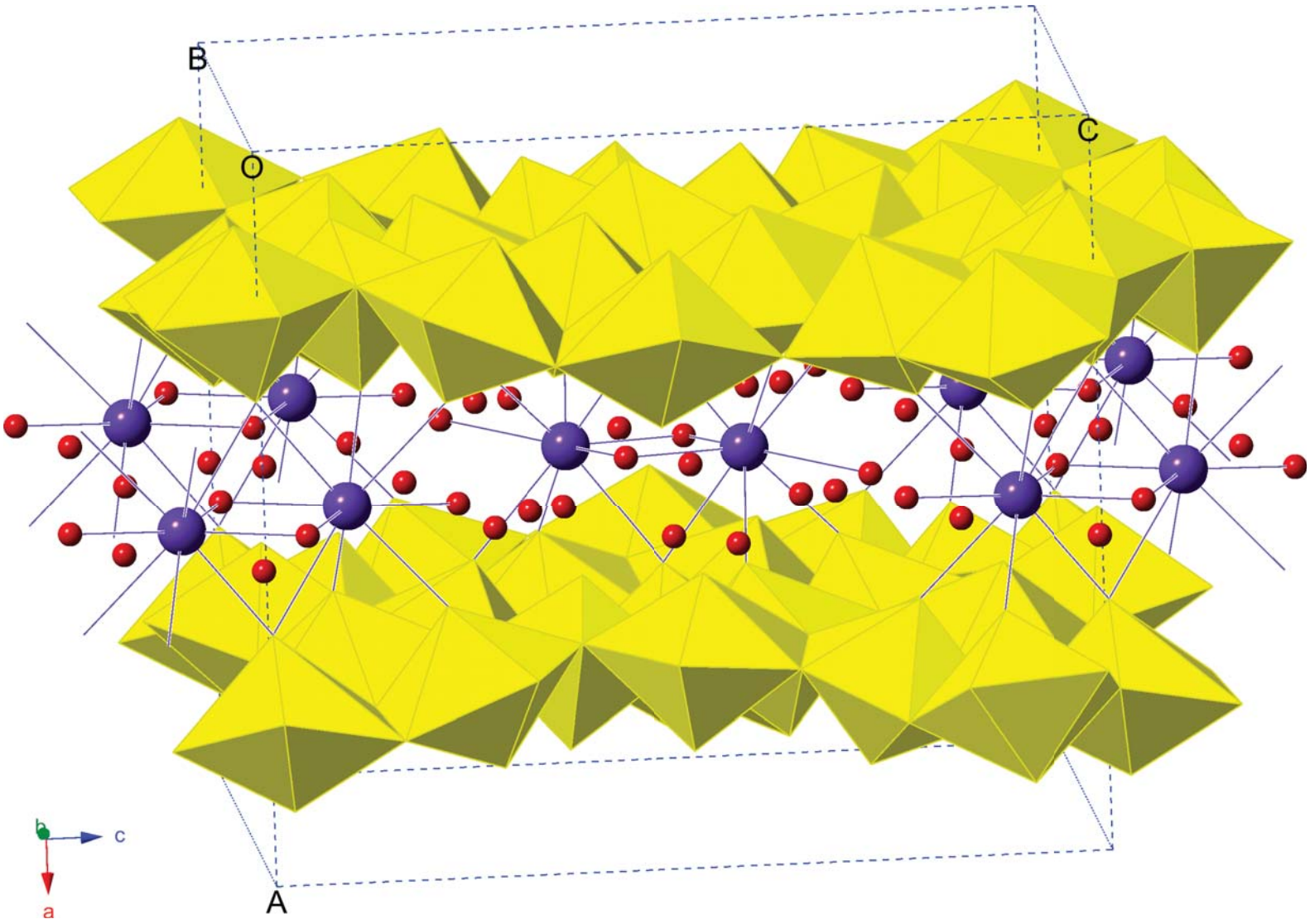

This is a preprint, the final version is subject to change, of the American Mineralogist (MSA)
Cite as Authors (Year) Title. American Mineralogist, in press.
DOI: http://dx.doi.org/10.2138/am-2018-6083

Figure 8

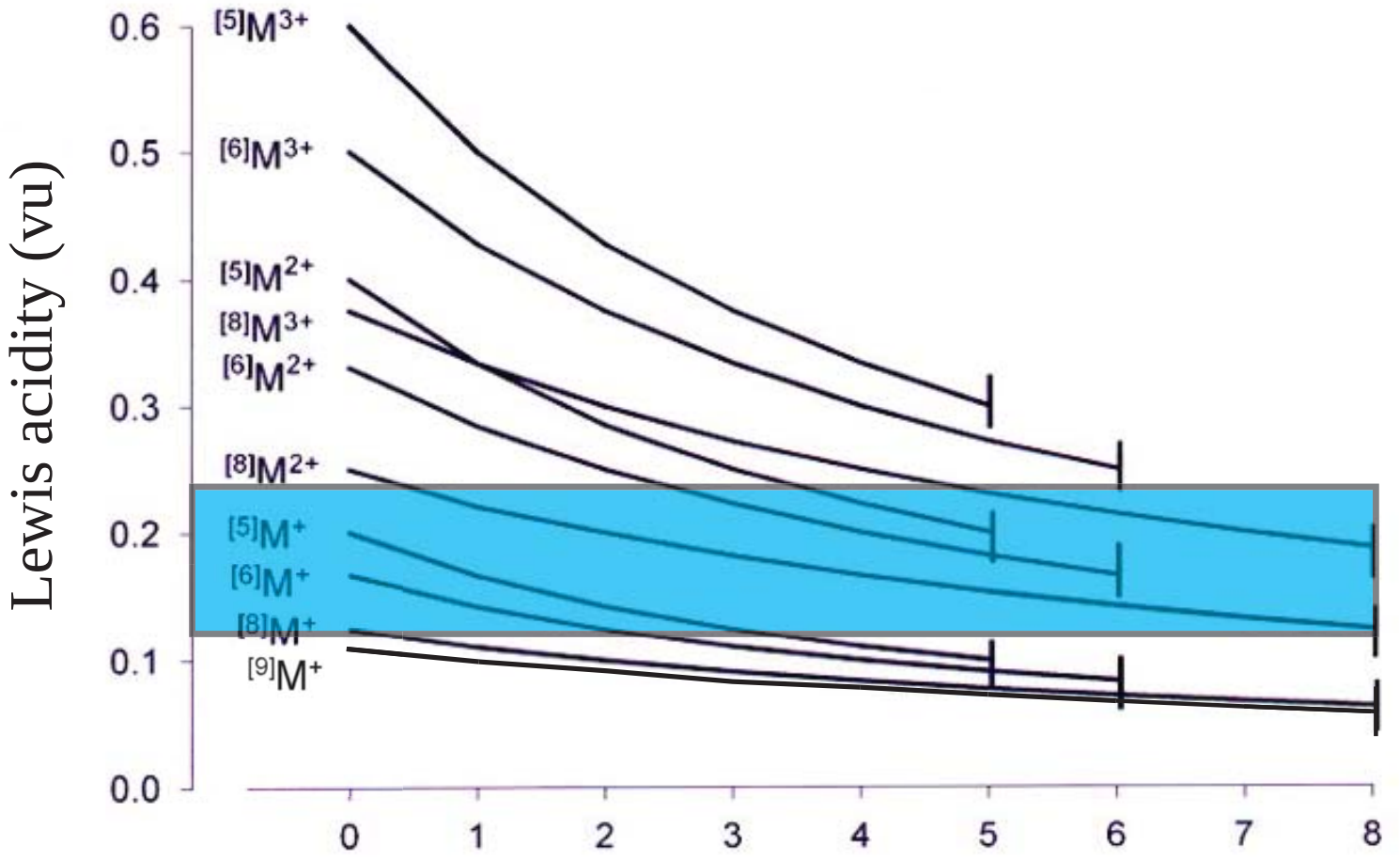

This is a preprint, the final version is subject to change, of the American Mineralogist (MSA)
Cite as Authors (Year) Title. American Mineralogist, in press.
DOI: http://dx.doi.org/10.2138/am-2018-6083

Table 1. Unit-cell parameters for analogous uranyl-oxide hydroxide hydrate phases.

Phase	*Occurrence*	*a* [Å]	*b* [Å]	*c* [Å]	*V* [Å^3]	*S.G.*	Σ_M *s.o.f.*
Neutral sheets							
schoepite[a]	Shaba, DRC	14.337(3)	16.813(5)	14.731	3426(7)	$P2_1ca$	0
metaschoepite[b]	Shaba, DRC	14.680(2)	14.029(2)	16.720(1)	3443	*Pbcn*	0
metaschoepite[c]	synthetic	14.6861(4)	13.9799(3)	16.7063(5)	3439	*Pbcn*	0
paraschoepite[d]	Shinkolobwe, DRC	14.12	16.83	15.22	3617	*Pbca*	0
heisenbergite[e]	Menzenschwand, DE	13.10(1)	13.76(1)	14.50(1)	2613.7(2)	$P2_12_12_1$;$Pna2_1$	0
paulscherrerite[f]	Radium Ridge, AU	4.288(2)	10.270(6)	6.885(5)	303.2(2)	$P2$;$P2_1$;$P2_1$/m	0
α-$UO_2(OH)_2$[g]	synthetic	4.242(1)	10.302(1)	6.868(1)	300.1(1)	*Cmca or C2cb*	0
Charged sheets							
leesite[h]	**Utah, USA**	**14.866(7)**	**14.126(7)**	**16.772(8)**	**3522(3)**	***Pbca***	**0.71**
Na-rich metaschoepite[i]	synthetic	14.7050(6)	14.0565(5)	16.7051(6)	3453	*Pbcn*	0.545
Na-rich metaschoepite[j]	Jáchymov, CZ	14.64(2)	14.03(1)	16.69(2)	3426(7)	*Pbcn*	0.91
K-rich fourmarierite[j]	Jáchymov, CZ	14.025(2)	16.469(4)	14.623(2)	3378(2)	$Bb2_1m$	0.96
K-rich fourmarierite[j]	Jáchymov, CZ	13.442(5)	16.611(6)	14.447(2)	3226(1)	$Bb2_1m$	1.03
fourmarierite[k]	Shinkolobwe, DRC	14.010(1)	16.401(1)	14.317(1)	3290	$Bb2_1m$	1.022
fourmarierite[k]	Shinkolobwe, DRC	14.018(1)	16.468(1)	14.368(1)	3317	$Bb2_1m$	0.863
fourmarierite[k]	synthetic	13.938(2)	16.638(3)	14.672(2)	3402	$Bb2_1m$	0.497
kroupaite[l]	Jáchymov, CZ	14.8201(8)	14.0958(8)	16.765(1)	3502.3(3)	*Pbca*	0.69

[a] Finch et al. (1996b), [b] Klingensmith et al. (2007), [c] Weller et al. (2000), [d] Schoep and Stradiot (1947), [e] Walenta and Theye (2012), [f] Brugger et al. (2011), [g] Taylor and Hurst (1971), [h] This work, [i] Klingensmith et al. (2007), [j] Sejkora et al. (2013), [k] Li and Burns (2000), [l] Plášil et al. (2017)

Table 2. LA-ICP-MS data (wt %) for leesite, average of 6 analyses.

Element	Mean Ratio (U/cation)	Range	SD	Mean *apfu*	Calculated wt% oxide
Na	0.001	0.0006-0.0014	0.0004	0.004	-
Ca	0.003	0-0.006	0.482	0.012	-
K	0.168	0.1632-0.1748	0.0042	0.670	2.4
U[a]	1.000	-	-	4	87.09 (as UO_3)
H_2O[b]	-	-	-		10.51

Notes: The element ratios above are alternatively expressed in calculated wt% oxide in the last column, based on the mean *apfu* derived from the count ratios for each element.
[a] Ratios normalized to 4 U *apfu*
[b] Calculated according to the structure with charge balance considerations on the basis of 20 O *apfu*

This is a preprint, the final version is subject to change, of the American Mineralogist (MSA)
Cite as Authors (Year) Title. American Mineralogist, in press.
DOI: http://dx.doi.org/10.2138/am-2018-6083

Table 3. Powder X-ray data (*d* in Å) for leesite.

I_{obs}	d_{obs}	d_{calc}	I_{calc}	*hkl*	I_{obs}	d_{obs}	d_{calc}	I_{calc}	*hkl*	I_{ob}	d_{obs}	d_{calc}	I_{cal}	*hkl*
		8.386	1	0 0 2			2.2690	1	0 2 7			1.743	1	1 8 1
92	**7.45**	7.433	100	2 0 0			2.2521	1	6 2 2	8	1.7214	1.717	3	2 8 0
		7.304	1	1 0 2			2.2340	1	4 0 6	7	1.6918	1.709	1	6 1 7
		6.509	2	0 2 1			2.2246	1	2 6 1			1.683	1	0 8 3
		5.402	1	0 2 2	5	2.216	2.1979	1	5 1 5			1.679	1	0 6 7
		5.077	1	1 2 2			2.1918	1	0 4 6			1.676	1	7 3 5
		4.897	1	2 2 1			2.1701	1	2 2 7			1.673	1	1 8 3
		4.504	3	3 1 1			2.1684	2	1 4 6			1.651	5	8 2 4
		4.370	2	2 2 2			2.1023	1	2 4 6	17	1.6507	1.644	3	8 4 0
		4.035	1	1 0 4	7	2.0955	2.0965	4	0 0 8			1.642	3	2 8 3
24	**3.713**	3.716	22	4 0 0			2.0838	2	7 1 1			1.638	2	2 6 7
		3.605	34	0 2 4			2.0529	9	0 6 4			1.632	1	9 1 1
65	**3.566**	3.586	1	3 1 3	**36**	**2.0431**	2.0420	11	6 2 4			1.631	1	0 2 10
		3.531	17	0 4 0			2.0283	5	6 4 0	6	1.6177	1.622	5	4 4 8
		3.366	1	1 4 1			2.0178	6	2 0 8			1.600	2	6 0 8
		3.344	1	3 3 1			2.0045	1	3 4 6	9	1.5909	1.594	1	4 8 0
		3.244	54	2 2 4			1.9917	1	1 2 8			1.593	2	2 2 10
100	**3.219**	3.227	1	4 2 1	**25**	**1.9817**	1.9788	10	2 6 4			1.580	3	6 6 4
		3.189	24	2 4 0			1.9750	2	4 6 1	5	1.5488	1.549	1	3 2 10
		3.133	1	2 4 1			1.9660	1	7 1 3			1.547	1	8 0 6
		3.061	1	4 2 2	5	1.9333	1.9366	1	4 2 7			1.533	1	4 8 3
		3.023	1	4 1 3			1.9232	1	7 3 1			1.530	1	4 6 7
		2.985	1	0 4 3			1.9111	1	1 6 5			1.494	1	4 2 10
		2.866	2	5 1 1			1.9067	1	6 4 3			1.486	1	10 0 0
5	2.825	2.795	1	0 0 6			1.8879	1	4 4 6	3	1.4544	1.457	2	6 4 8
		2.770	3	2 4 3			1.8625	1	3 2 8			1.438	1	6 8 0
		2.747	1	1 0 6	5	1.8601	1.8583	3	8 0 0			1.433	1	10 2 2
		2.616	1	2 0 6			1.8542	1	6 0 6			1.417	1	8 4 6
		2.599	1	0 2 6			1.8293	1	7 3 3			1.401	1	8 3 7
		2.587	15	4 2 4			1.8260	4	4 0 8	3	1.4026	1.392	1	6 8 3
28	**2.578**	2.560	9	4 4 0	**18**	**1.8009**	1.8028	4	0 4 8			1.390	1	8 0 8
		2.486	1	1 5 3			1.7970	7	4 6 4			1.390	1	6 6 7
5	2.491	2.477	4	6 0 0			1.7658	1	0 8 0			1.383	1	2 10 1
		2.453	1	2 2 6			1.7572	1	8 2 2			1.377	2	8 6 4
		2.331	2	0 6 1	9	1.7602	1.7520	5	2 4 8	9	1.3765	1.374	3	10 2 4
9	2.314	2.292	1	5 3 3			1.7498	1	8 1 3			1.371	1	0 2 12
												1.370	1	10 4 0

This is a preprint, the final version is subject to change, of the American Mineralogist (MSA)
Cite as Authors (Year) Title. American Mineralogist, in press.
DOI: http://dx.doi.org/10.2138/am-2018-6083

Table 4. Bond-valence analysis (valence units, *vu*) for leesite.

	U1	U2	U3	U4	K1	Σ	O assignment	Expected H-bonds
O1	1.71					1.70	yl O	(0.2 x 1)
O2	1.72				0.15	1.87	yl O	(0.2 x 1)
O3	0.49	0.40		0.42		1.32	OH	(0.8 x 1)
O4	0.73		0.68	0.69		2.10	O	
O5		1.71			0.10	1.81	yl O	(0.2 x 1)
O6		1.75			0.13	1.88	yl O	(0.2 x 1)
O7	0.38	0.47	0.44			1.30	OH	(0.8 x 1)
O8	0.65	0.61				1.26	OH	(0.8 x 1)
O9		0.74	0.68	0.64		2.07	O	
O10		0.48	0.31	0.51		1.29	OH	(0.8 x 1)
O11			1.65			1.65	yl O	(0.2 x 2)
O12			1.71		0.08, 0.08	1.86	yl O	(0.2 x 1)
O13	0.48		0.49	0.38		1.35	OH	(0.8 x 1)
O14				1.67	0.13	1.79	yl O	(0.2 x 1)
O15				1.67		1.67	yl O	(0.2 x 2)
Ow1					0.23, 0.12	0.35	H_2O	(0.8 x 2)
Ow2						0.00	H_2O	(0.8 x 2) + (0.2 x 2)
Ow3					0.08	0.08	H_2O	(0.8 x 2) + (0.2 x 2)
Ow4						0.00	H_2O	(0.8 x 2) + (0.2 x 2)
Ow5						0.00	H_2O	(0.8 x 2) + (0.2 x 2)
Σ	6.17	6.17	5.96	5.99	1.10			

Notes: Bond-valence parameters for U^{6+}-O taken from Burns et al. (1997a), K^{+}-O taken from Wood and Palenik (1999). All strengths are calculated assuming full site occupancy (K). Predicted hydrogen bond-valence contributions to each atom are included, with values for donor (D—H, ~0.8 *vu*) and acceptor (H—A, ~0.2 *vu*) bond strengths taken from Hawthorne and Schindler (2008).